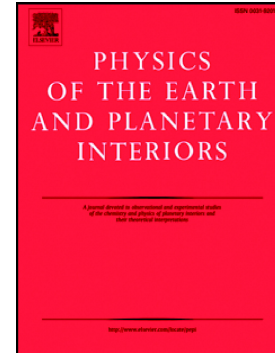


Extremely young melt infiltration of the sub-continental lithospheric mantle

Simon Turner, Michael Turner, Bernard Bourdon, Kari Cooper, Don Porcelli



PII: S0031-9201(19)30034-2

DOI: <https://doi.org/10.1016/j.pepi.2019.106325>

Reference: PEPI 106325

To appear in:

Received date: 2 February 2019

Revised date: 10 September 2019

Accepted date: 3 October 2019

Please cite this article as: S. Turner, M. Turner, B. Bourdon, et al., Extremely young melt infiltration of the sub-continental lithospheric mantle, (2019), <https://doi.org/10.1016/j.pepi.2019.106325>

This is a PDF file of an article that has undergone enhancements after acceptance, such as the addition of a cover page and metadata, and formatting for readability, but it is not yet the definitive version of record. This version will undergo additional copyediting, typesetting and review before it is published in its final form, but we are providing this version to give early visibility of the article. Please note that, during the production process, errors may be discovered which could affect the content, and all legal disclaimers that apply to the journal pertain.

Extremely young melt infiltration of the sub-continental lithospheric mantle

Simon Turner^{1*}, Michael Turner¹, Bernard Bourdon², Kari Cooper³, Don Porcelli⁴

¹Department of Earth and Planetary Sciences, Macquarie University, Sydney, Australia

²Laboratoire de Géologie de Lyon, CNRS, UMR 5276, Ecole Normale Supérieure de Lyon, France

³Department of Earth and Planetary Sciences, University of California, Davis, USA

⁴Department of Earth Sciences, University of Oxford, United Kingdom

*Corresponding author

E-mail address: simon.turner@mq.edu.au (S. Turner)

ABSTRACT

It has long been inferred that mantle metasomatism and the incompatible element enrichment of the continents both require movement of melts formed by very low degree melting of the mantle. Yet establishing the presence of these melts and whether this process is on-going and continuous, or spatially and temporally restricted, has proved difficult. Here we report large U-Th-Ra disequilibria in metasomatised, mantle xenoliths erupted in very young lavas from the Newer Volcanics Province in southeastern Australia. The ^{226}Ra - ^{230}Th disequilibria appear to require reappraisal of previous estimates for the age of eruption that now seems unlikely to be more than a few kyr at most. We propose that infiltration of carbonatitic melts/fluids, combined with crystallization of pargasite, can account for the first order U-series disequilibria observations. Irrespective of the exact details of the complex processes responsible, the half-lives of the nuclides require that some of the chemical and isotopic disturbance was extremely young ($\ll 8$ kyr) and potentially on-going at the time of incorporation into the alkali basalts that transported the xenoliths to the surface. This provides evidence for the presence and possibly continuing migration of small melt fractions ($\sim 0.02\%$) in the upper convecting mantle that may contribute to the seismic low velocity zone. By implication, it appears that the asthenosphere must lie close to its solidus, at least in this region. Pressure-temperature estimates indicate that the small degree melts identified could infiltrate as far as 25 km upwards into the sub-continental lithospheric mantle leading to strong incompatible element enrichment and the recent timing of this event this urges a reappraisal of the meaning of 300-500 Ma Nd model ages in mantle xenoliths from this region. In principle, the resultant metasomatised mantle could provide a component for some ocean island basalts, should the sub-continental lithospheric mantle be returned to the asthenosphere by convective removal at some later time.

Keywords: sub-continental mantle lithosphere; metasomatism; U-series ages; carbonatite; seismic low velocity zone

Journal Pre-proof

1. Introduction

A long-standing and important, yet largely untested, tenet holds that differentiation of the Earth and formation of the continents has occurred via multistage processes which, at some point, involves a very small ($< 1\%$) melt fraction (O’Nions and McKenzie, 1988). In principle, such melts might be present everywhere in the upper mantle and, if so, could continuously infiltrate and chemically modify the sub-continental lithospheric mantle at the base of the tectonic plates (McKenzie, 1989) in a process broadly referred to as mantle metasomatism. These melts cannot constitute a major advective heat or mass flux, yet they could be important in determining the final trace element and radiogenic heat budget of the sub-continental lithospheric mantle and perhaps, ultimately, the continents. In the underlying asthenosphere, small melt fractions have long been invoked as agents of metasomatism that can result in large time-integrated, radiogenic isotopic anomalies relative to the bulk silicate Earth (e.g., DePaolo and Wasserburg, 1976). It has also been suggested that, should the lower parts of metasomatised, sub-continental lithospheric mantle or oceanic upper mantle become removed by convection, such material might eventually re-emerge at the Earth’s surface as a component of ocean island basalts (McKenzie and O’Nions, 1983; Workman et al. 2004).

Experimental studies suggest that at depths less than 200 to 250 km the adiabatically convecting upper mantle lies close to its solidus in the presence of small amounts of H_2O and/or CO_2 (Green et al., 2010) and the small melt fractions (0.02-0.1%) that might exist as a consequence have been proposed as one explanation for the existence of the seismic low velocity zone (see Karato and Jung, 1998; Hirschmann, 2010). Unfortunately, such models remain very hard to test. It has been argued that alkali basalts erupted through the Pacific plate as it bends and cracks on approaching the Japan trench provide evidence for the on-going presence of melt in the asthenosphere (Hirano et al., 2006). However, those magmas reflect significantly larger accumulated degrees of melting than discussed above and, because small melt fractions of

relevance to this discussion cannot yet be studied experimentally (Zhu et al., 2010), there has been little opportunity to verify if and how they might be involved in the differentiation within the mantle. Here we report the results of a U-series isotope approach designed to provide new age constraints that might help to address some of these substantive issues. Because U-Th-Ra disequilibria are preserved only on timescales of 1,000's to 100,000's years they can reveal whether trace element disturbance (metasomatism) occurred very recently, whether this involved very small melt fractions that could be significant for seismic-wave travel times, and whether such metasomatism would impart extreme incompatible trace element enrichment that could be significant for long-term chemical differentiation of the Earth's mantle.

2. Sampling of the southeast Australian sub-continental lithospheric mantle

Mantle xenoliths erupted in volcanic rocks provide rare but direct glimpses into the processes of metasomatic enrichment of the sub-continental lithospheric mantle (e.g., Menzies and Murthy, 1980). U-series isotopes afford a unique means to assess this metasomatism since fractionation between the different nuclides is only possible at extremely low degrees of melting or during reactive porous flow and the resultant disequilibria returns to secular equilibrium over timescales < 500 kyr (see Bourdon et al., 2003, for a review). Thus, they provide information that can help answer key questions concerning the melt fractions and time scales (and thereby physical mechanisms) involved in these processes. Although most intra-plate xenoliths are too old for this approach, the Newer Volcanic province of southeast Australia (Figs. 1a, b) has brought xenoliths to the surface in lavas that are likely to be at least as young as 4 kyr (Price et al., 2003; see also below). This region represents one of the classic areas for the study of both intra-plate, alkali basalts (Frey et al., 1978; Demidjuk et al., 2007; Davies and Rawlinson, 2014) and metasomatised xenoliths (e.g., Griffin et al., 1984; McDonough and McCulloch, 1987; Stolz and Davies, 1988;

Yaxely et al., 1998) and it is arguably one of the very few places on Earth where the hypothesis of on-going mantle metasomatism can be tested using U-series isotopes.

Subchondritic $^{187}\text{Os}/^{188}\text{Os}$ isotope ratios in xenoliths from this region indicate that the southeastern Australian sub-continental lithospheric mantle was once strongly depleted by melt extraction and T_{DM} model ages indicate that this probably occurred in the Meso-Neoproterozoic (McBride et al., 1996; Handler et al., 1997). This melt extraction would have left behind refractory harzburgites or dunites (Frey and Green, 1974) and most studies of the xenoliths have inferred subsequent enrichment by one or more metasomatic episodes (e.g., Griffin et al., 1984; Stolz and Davies, 1988; Yaxely et al., 1998). Nd isotope model ages have been used to infer that incompatible trace element enrichment occurred in the xenoliths ~300-500 Myr ago (Griffin et al., 1988). Clearly, if this age range were correct, all of the U-series nuclide pairs should now be in U-series isotopic equilibrium.

Although our purpose is to place new constraints on the timing of youngest metasomatism, numerous previous studies have documented that at least one metasomatic episode recorded by the western Victorian xenoliths involved carbonatitic melts (Green and Wallace, 1988; Yaxely et al., 1998). Thus, in addition to modal metasomatic phases like amphibole (Figs. 1b,c), the minerals in the xenoliths are characterised by trails of melt and fluid inclusions that are CO_2 -rich (Fig. 1c). Unfortunately, the melt inclusions in the xenoliths are typically either too small to analyse or else contain other phases (e.g., spinel) that compromise their utility to record infiltrating melt compositions. However, Yaxley et al. (1998) reported three successful analyses of melt inclusions; two are silicic melts and one is carbonatite indicating that both silicic and carbonatitic metasomatism have affected these rocks. The fluid inclusions have asthenospheric noble gas and C isotopic signatures (Porcelli et al., 1992; Matsumoto et al., 2000). They also have high U and Th contents and the observations of nucleogenic Ne coupled with the absence of ^4He accumulation indicate open-system behaviour with apparent ^{21}Ne accumulation ages of 3 to 11 Ma. This indicates that 90% of accumulated Ne must have been lost recently either due to recent heating or because the

metasomatism responsible for U-Th enrichment took place in the past few Ma (Matsumoto et al., 2000). Similarly, the apparent absence of in-situ produced ^{40}Ar in the amphiboles indicates that the hydrous phases are very young (Matsumoto et al., 2000).

3. Materials analysed

In this study, we analysed U-series isotopes in mineral separates from two amphibole-bearing, spinel lherzolite xenoliths from the Lake Bullenmerri (BM993) and Lake Gnotuk (GN9911) maars (Fig. 1a) chosen from the collection of Powell et al. (2004). These two maars have generally been inferred to be monogenetic and potentially up to 8000 yrs old (DeDeckker, 1982; Price et al., 2003). However, there is good field and geophysical evidence for several episodes of eruption at each locality (van Otterloo et al., 2014; R. Cas, personal communication) and some ^{14}C ages and palaeomagnetic data in the province are only a few kyr old (Blackburn et al. 1982; Barbetti & Sheard 1981). The xenoliths from these two maars have been the subject of a number of detailed petrological studies (Griffin et al., 1984; Stolz and Davies, 1988) and we selected two on the basis of their high modal (and thus analysable) amphibole content as well as a visual lack of interstitial glass resulting from decompression melting of the hydrous minerals (cf. Yaxley et al., 1998) that might complicate determination of the age of the youngest metasomatism in this region.

The specific xenoliths analysed are apatite-free, have been described in detail by Powell et al. (2004) and are broadly similar to other xenoliths from the region. GN9911 is more depleted in trace elements than BM993. They contain a mild foliation defined by alignment of clusters of amphibole (Fig. 1b) and have porphyroclastic to mosaic granoblastic microstructures in which amphibole forms discrete grains (Fig. 1c). Sample BM993 comprises 60% olivine, 17% orthopyroxene, 6% clinopyroxene and 17% amphibole (low-Ti pargasite) with minor spinel. Sample GN9911 consists of 61% olivine, 23% orthopyroxene, 8% clinopyroxene, 6% amphibole (low-Ti pargasite) and 2% spinel. Note that these minerals are not in Sr-Nd-Pb isotopic equilibrium

(Stolz and Davies, 1988; Powell et al., 2004). Major and trace element analyses of the bulk xenoliths and representative constituent minerals from Powell et al. (2004) are given in Table 1 with phase equilibria suggesting oxygen fugacities around -1 relative to the QFM buffer (Powell et al., 2004). Applying equations 36 and 38 from Putirka (2008) to the mineral data reported by Powell et al. (2004) we obtained equilibration temperatures and pressures of 900-940 °C and 1.13-1.19 GPa, respectively. These suggest depths of last equilibration at around 40 km depth based on the geotherm of Griffin et al. (1984). Although the lack of isotopic equilibrium between the mineral phases might cast doubt on the utility of geothermometry the inferred conditions are consistent with experimental data obtained on associated garnet proxenite xenoliths (Adam et al., 1992). The inferred depth places the origin of the xenoliths about 25 km above the base of the continental lithosphere (~ 65km) in this region (Fishwick et al., 2008; Ford et al., 2010). Both xenoliths are strongly enriched in incompatible trace elements (Fig. 2) and have radiogenic isotope signatures that are distinct from their host basalts, precluding a common origin (e.g., McDonough and McCulloch, 1987).

In addition, we undertook analysis of a host tuff from Lake Bullenmerri and basaltic material adhering to a xenolith similar to BM993 from the same locality. The Bullenmerri basalt is a *ne-mugearite*, identical in most respects to lavas erupted at Mount Gambier and Mount Schank (Frey et al., 1978; McDonough and McCulloch, 1987; Price et al., 2003; Demidjuk et al., 2007). The analysis of the Gnotuk host lava in Table 1 is taken from Stolz and Davies (1988); other major and trace element data are taken from Powell et al. (2004).

4. Analytical methods

Slabs were cut from the interiors of two large (~15 cm diameter) xenoliths to remove any possible exterior alteration rinds. They were then crushed to ~ 0.5-1 mm sized grains in a stainless-steel disk-mill after which bulk mineral separates were obtained using standard Franz magnetic

techniques. Multiple aliquots of clinopyroxene, orthopyroxene and amphibole were hand picked under a binocular microscope over the course of the project. All separates were washed in milli-Q water prior to analysis and the original bulk U-Th-Ra isotope analyses were performed at Macquarie University in 2005. The host basalt and tuff samples were crushed and powdered in an agate mill in 2012 and analysed following standard x-ray fluorescence and inductively-coupled, plasma mass spectrometry methods (see Firth et al., 2016 for details).

A significant proportion of the grains from the mineral separates contain trails of $< 50 \mu\text{m}$ melt and fluid inclusions that cross-cut the assemblages and have negative crystal shapes (Powell et al., 2004; Andersen et al., 1984). Unfortunately, these inclusions are too small for individual analysis. Hence, in order to place some constraints on their composition, we exploited the heterogeneity of the mineral separates to try to isolate the effect of the metasomatic component represented by the inclusions. Following the approach of Rosenbaum et al. (1996), this was achieved by comparing analyses of relatively inclusion-free separates with the bulk analyses that include the contributions from the inclusions. The relatively inclusion-free separates were obtained by hand-picking under a binocular microscope and these were analysed in 2010. The bulk clinopyroxenes were also re-analysed in 2012 to further assess the heterogeneity of the grains. In addition to the analysis of the bulk Gnotuk orthopyroxene, we also analysed a second bulk orthopyroxene separate in 2012 that had been leached by ultrasonication in cold 6M HCl for 10 minutes and analysed both this leachate and the solid residue.

In view of the variable and sometimes extreme disequilibria observed, further aliquots of clinopyroxene and orthopyroxene from the Gnotuk xenolith were hand picked in 2017 and analysed at the University of California, Davis in 2018. Prior to shipping the orthopyroxene was leached cold 6M HCl for 10 minutes whereas the clinopyroxene was only washed in milli-Q water.

4.1. Analysis at Macquarie University

All materials the above were weighed (typically 0.2-1g) and spiked with ^{236}U - ^{229}Th and ^{228}Ra tracers prior to dissolution in heated Teflon pressure vessels using a HF-HNO₃-HCl mix of Teflon-distilled acids. Residual fluorides were removed using HClO₄ and H₃BO₃. Complete dissolution of the mineral separates, including grains of spinel, was achieved by prolonged, cyclical attack with concentrated HCl, HNO₃ and aqua regia.

The final product was converted to nitrate using 14N HNO₃ and then taken up in 7N HNO₃. U and Th purification was achieved via a single pass through a 4 ml anionic resin column using 7N HNO₃, 6N HCl and 0.2N HNO₃ as elutants. We purposefully avoided the use of EiChrom® resins for the U-Th chemistry as these can bleed organic molecules that lead to memory effects and interferences during analysis. Concentrations and isotope ratios were measured in dynamic mode on a Nu Instruments® multi-collector, inductively-coupled plasma mass spectrometer. ^{238}U and ^{235}U were analysed on Faraday cups, using the $^{238}\text{U}/^{235}\text{U}$ ratio to determine the U mass bias, assuming $^{238}\text{U}/^{235}\text{U} = 137.88$, whilst ^{236}U and ^{234}U were alternately collected in the IC0 ion counter that is preceded by an energy filter. The IC0 gain was determined during interspersed dynamic analyses of the CRM145 standard assuming a $^{234}\text{U}/^{238}\text{U}$ ratio of 5.286×10^{-5} (Cheng et al., 2000). Methods for Th isotope measurements employed a dynamic routine with ^{232}Th in Faraday cups and ^{230}Th and ^{229}Th alternating on IC0 and using bracketing measurements of the Th"U" standard (Open University Th solution) to obtain the Th mass bias which can be up to 4% different to that for U. Measurements at masses 230.5 and 229.5 were used to derive a linear correction for residual ^{232}Th tail interference as described in detail for these laboratories by Sims et al. (2010). For our setup, application of a polynomial tail correction can lead to a $\leq 0.6\%$ lower $^{230}\text{Th}/^{232}\text{Th}$ ratio. Typical within run errors on $^{234}\text{U}/^{238}\text{U}$ and $^{230}\text{Th}/^{232}\text{Th}$ ratio measurements yielded values of 2.61×10^{-8} and 1.10×10^{-8} , respectively.

The Ra analysis procedure follows that used by Turner et al. (2000). Ra was taken from the first elution from the anionic column and converted to chloride using 6N HCl. This was then loaded in 3 N HCl onto an 8 ml cationic column and Ra, Ba and the rare earth elements (REE) eluted using

3.75M HNO₃. The process was repeated on a scaled-down 0.6 ml column. The REE were then removed using a 150 µl column of EiChrom® Ln-spec resinTM and 0.1N HNO₃. Ra and Ba were finally chromatographically separated using EiChrom® Sr-spec resinTM and 3N HNO₃ as elutant in a 150 µl procedure. Samples were loaded onto degassed Re filaments using 1-2 µl of a Ta-HF-H₃PO₄ activator solution (Birck, 1986) and ²²⁸Ra/²²⁶Ra ratios were measured to a precision ≤ 1 % in dynamic ion counting mode on the central cup of a ThermoFinnigan Triton® thermal ionisation mass spectrometer. Organic interferences are often noted at low temperatures during analysis of Ra but were minimised here by using the instrument fitted with a dry scroll pump instead of the standard rotary pump. This modification helps prevent leakage of organic molecules into the source during venting, though some are residual from the Sr-spec resin.

4.2. Analysis at University of California, Davis

Splits of GN9911 clinopyroxene and leached orthopyroxene were analyzed at UC Davis in 2018. Separates of ~1 g were washed in 18 megaohm (milli-Q) water prior to dissolution and analysis. The separates were dissolved in a concentrated HF-HNO₃ mixture (3:1 HF:HNO₃, using acids distilled twice at sub-boiling conditions in Teflon stills). Residual fluorides were attacked using saturated boric and perchloric acids. A small fraction of spinel grains (likely inclusions) remained after the dissolution, but the amount was too small to measurably affect the reported ratios and concentrations of U-series nuclides. The final solutions were split into two aliquots, one spiked with a ²²⁹Th-²³³U tracer and used for isotope dilution measurements of U and Th concentrations, and the second (larger) split was spiked with a ²²⁸Ra tracer and was used for measurements of U and Th isotopic compositions and isotope dilution measurement of Ra concentrations. The ²³³U-²²⁹Th tracer was prepared from an NSF-supported stock of ²²⁹Th combined with ²³³U originally obtained by B. Nelson at University of Washington, and was calibrated using a combination of secular-equilibrium rock standards and NIST Th and U concentration standards (SRM 3159 Th

standard, and SRM 3164 U standard). The ^{228}Ra tracer was prepared by chemically separating radium from a thorium solution prepared from Ames thorium metal at UC Davis in 2009. The ^{228}Ra concentration of the tracer was calibrated using SRM 4965 ^{226}Ra solution, and the isotopic composition of the tracer was calibrated using repeated measurements on a *Nu Instruments*® multi-collector, inductively-coupled plasma mass spectrometer. The concentration and isotopic composition of the tracer at the time of analyses was calculated by correcting for decay using a half-life for ^{228}Ra of 5.75 years (Holden, 1990). Decay-corrected isotopic composition of the tracer has remained stable since initial calibration (decay-corrected $^{226}\text{Ra}/^{228}\text{Ra} = 1.178 \pm 0.001$, 2 standard deviations of the mean, $n=15$), indicating that the amount of residual ^{232}Th in the tracer solution is negligible. Analyses of rock standard W-2 run in parallel with the separates yielded ($^{230}\text{Th}/^{238}\text{U}$) = 1.010 and ($^{226}\text{Ra}/^{230}\text{Th}$) = 0.954, providing a measure of the accuracy of the combined measurements. Long-term averages of repeated measurements of rock standards W-2, BCR-2 and AGV-2 are within 0.5% of secular equilibrium for ($^{230}\text{Th}/^{238}\text{U}$) ratios and within 2% of secular equilibrium for ($^{226}\text{Ra}/^{230}\text{Th}$).

Th and U in the isotope dilution aliquots were purified using TRU resin using procedures detailed in Cooper and Donnelly (2008). The Th and U fractions for isotopic composition measurements were separated from the larger sample aliquot using TRU resin, and the initial wash fractions were saved for radium. Radium was separated from major and most trace elements using cation-exchange resin, followed by Ra-Ba separation using Sr-spec resin, as detailed in Cooper and Donnelly (2008). Total-process blanks for this batch of chemistry were $<11 \text{ pg } ^{238}\text{U}$, $<1 \text{ pg } ^{232}\text{Th}$, and ^{226}Ra below detection ($<0.1 \text{ fg}$). Blanks were subtracted before calculation of concentrations, with negligible effects on the measured concentrations.

Measurements were performed on a *Nu Instruments*® multi-collector, inductively-coupled plasma mass spectrometer using procedures slightly modified from those in Cooper and Donnelly (2008). Briefly, U and Th concentrations by isotope dilution were calculated from measurements of $^{233}\text{U}/^{238}\text{U}$ and $^{229}\text{Th}/^{232}\text{Th}$ analyzed separately using static routines on Faraday cups. Mass bias was

calibrated using measurements of NIST CRM 112A before analyses of unknowns and interspersed between every 3-4 unknowns. Uranium isotopic compositions were measured using a static analysis routine with ^{238}U and ^{235}U measured on Faraday cups and ^{234}U measured on an ion multiplier. Instrumental mass bias and Faraday-ion counter gain were calibrated using NIST CRM 112A. The procedure for Th isotopic composition measurement was modified from that in Cooper and Donnelly (2008) by using thorium isotopic standard IRMM-036 to calibrate instrumental mass bias and Faraday-ion counter gains. ^{232}Th tailing below the ^{230}Th peak was corrected using an exponential fit to the shape of the tailing observed in analysis of Th standard WUN on the same day, combined with measurements at masses 229.5 and 230.5 for each sample.

4.3. Analytical uncertainty

Results from analyses of the rock standard TML-3 during the associated periods of analysis at Macquarie University are listed in Table 2 and a detailed inter-laboratory comparison for Th isotopes is provided in Sims et al. (2008). Total procedural blanks were < 50 pg for U and Th and below the detection limit for Ra ($\sim 0.1 \text{ fg} \cdot \text{g}^{-1}$). Results for rock standard W-2 at UC Davis are presented in Table 3. For details on results for other standard reference materials see Turner et al. (2011) who adopted 2 standard deviation precisions of 8 % for ($^{234}\text{U}/^{238}\text{U}$), 2 % for ($^{238}\text{U}/^{232}\text{Th}$), 1 % for ($^{230}\text{Th}/^{232}\text{Th}$), 2 % for ($^{230}\text{Th}/^{238}\text{U}$) and 6 % for ($^{226}\text{Ra}/^{230}\text{Th}$) for the TML data. However, we accept that the rock standards have orders of magnitude more U, Th and Ra than the minerals analysed in this study and so these precisions may be less applicable to the current study. However, we have regularly analysed similarly low concentrations materials (e.g., Turner et al., 1997, 2000, 2011) including other mantle peridotites (Turner et al., 2012). Moreover, we find no tendency towards larger disequilibria with decreasing concentration as might be expected if the disequilibria were an analytical issue that is exacerbated in low concentration materials (Fig. 3). Thus, to the best

of our knowledge we believe that the disequilibria are real and proceed with the following discussion on that basis.

5. Results and assessment of mineral heterogeneity

The Macquarie University results are presented in Table 2 and the UC Davis results in Table 3. The half-lives of the nuclides used to calculate the activity ratios were those compiled in Bourdon et al. (2003). Due to the uncertainty in ages of all the materials, no age corrections were applied to any of the data. The Bullenmerri host tuff is in U-Th secular equilibrium whereas the basalt adhering to one of the Bullenmerri xenoliths has large ^{230}Th excess. This is consistent with the field evidence that the tuff is older than the basalt-xenolith pair and it provides further evidence that these centres were subject to multiple magma injections (van Otterloo et al., 2014; Ray Cas, personal communication). Both samples have $\sim 7\%$ ^{226}Ra - ^{230}Th disequilibria that are similar to the small amount of disequilibria found in U-series analyses of alkali lavas erupted at Mount Gambier and Mount Schank (Demidjuk et al., 2007).

The mineral separate data reveal several important features but it appears that that most of the minerals exhibit significant U-series disequilibria, often including ^{234}U - ^{238}U disequilibria (discussed below). For example, ($^{230}\text{Th}/^{238}\text{U}$) ratios range from 0.49 to 1.53. Moreover, disequilibria is not only observed between ^{238}U and ^{230}Th (half-life 75 kyr) but also between ^{230}Th and ^{226}Ra (half-life 1600 yr) with ($^{226}\text{Ra}/^{230}\text{Th}$) ratios ranging from 0.12 to 9.7. These latter disequilibria represent some of the largest ever measured and this is remarkable, given that the host lavas have till now been inferred to be at least several kyr old. It raises the possibility that the ^{14}C ages may have been influenced by influx of “old” carbon and this requires further investigation.

Previous studies have clearly demonstrated that the minerals from these xenoliths show significant chemical heterogeneity (e.g., Stolz and Davies, 1988; Powell et al., 2004) and therefore we fully expected analyses of different mineral aliquots to yield variable bulk U-series

compositions. We believe this has been exacerbated by picking multiple separates at different times (cf. Tables 2 versus 3). With this caveat in mind, the data from the initial separates reported in Table 2 show that the two bulk clinopyroxene analyses for BM993 are similar in composition. In contrast, the GN9911 clinopyroxene is more heterogeneous with respect to both U-Th and Th-Ra disequilibria. The sense of disequilibria (i.e. ^{230}Th excess combined with ^{226}Ra deficit) was reproduced in multiple dissolutions of the same separate for the clinopyroxenes from both xenoliths. In addition, the large ^{226}Ra excess reproduced between analyses of two different analyses of the same separate of the Gnotuk orthopyroxenes (Table 2). However, the UC Davis data from a subsequent mineral picking yielded some contrasting results (Table 3). This GN9911 clinopyroxene separate appears close to equilibrium but the leached orthopyroxene has significant ^{230}Th deficit combined with ^{226}Ra excess. We also note that the U-Th data for the leached orthopyroxene and the leachate in Table 2 do not mass balance to the un-leached orthopyroxene. However, these analyses were necessarily made on different aliquots of orthopyroxene and so this may also reflect the gross heterogeneity of the grains and variable presence of inclusions.

If we accept that there are major heterogeneities, most of the minerals appear to have significant U-Th and Th-Ra disequilibria and even a ($^{226}\text{Ra}/^{230}\text{Th}$) ratio of 2 (i.e. 100% ^{226}Ra excess) must have been generated within the last few kyr. Before we consider the U-Th-Ra isotope data further, we first discuss the range in measured ($^{234}\text{U}/^{238}\text{U}$) ratios.

5.1. ^{234}U - ^{238}U disequilibria

A point of note is that many of the analyses have ($^{234}\text{U}/^{238}\text{U}$) ratios that are beyond likely analytical error of secular equilibrium. We cannot rule out that this may in part reflect interaction with a low temperature surficial component and/or alteration but consider such processes insufficient to explain all of the disequilibria because (1) the separates comprised only visually fresh grains, (2) no difference in $^{86}\text{Sr}/^{86}\text{Sr}$ has been found between leachates and residues of mineral

separates in previous studies (Stolz and Davies, 1988) suggesting negligible post-entrapment contamination of the xenoliths, (3) ($^{234}\text{U}/^{238}\text{U}$) ratios both greater and less than 1 are observed whereas surface waters are ubiquitously enriched in ^{234}U (e.g., Chabaux et al., 2003), (4) the leachate from the orthopyroxene did not have significantly higher ($^{234}\text{U}/^{238}\text{U}$) than many of the other analyses, and (5) there is no correlation between ($^{234}\text{U}/^{238}\text{U}$) and either U-Th or Ra-Th disequilibria (Fig. 4).

Cooper (2001) also reported ($^{234}\text{U}/^{238}\text{U}$) disequilibria (up to 1.6%) in mineral separates from a cumulate peridotite xenolith from Hawaii. Thus, it appears that some intrinsic process, perhaps specific to xenoliths, results in fractionation of ^{234}U from ^{238}U . One possibility is that this reflects recoil effects into or out of inter-granular films. It is well known that the minerals in mantle xenoliths are commonly coated in a former melt-like phase as documented by a deficit between individual mineral analyses and bulk xenolith analyses for incompatible elements (Jagoutz et al., 1980). Inter-granular films are inferred to be only μm 's thick - approaching the recoil distance ($\sim 20\text{-}25\text{ nm}$) for ^{238}U that could both accumulate in, and become lost from, this material. It is important to note that such films are distinct in both size and origin from the small patches of glass resulting from amphibole breakdown during ascent to the surface (Yaxley and Kamenetsky, 1999).

For the xenoliths analysed here, BM993 has 0.55 ppm Th and 0.12 ppm U that can be compared with that obtained by mass balance of the relatively inclusion-free mineral compositions using the modes given above. This calculation predicts 0.39 ppm Th and 0.07 ppm U and the same calculation performed for GN9911 (which has 0.10 ppm Th, 0.03 ppm U) yields 0.07 ppm Th and 0.02 ppm U. Thus, both bulk xenoliths contain approximately double the Th and U contents obtained by mass balance calculations. This could be consistent with either (1) heterogeneity arising from the inclusions, (2) the presence of an unobserved trace phase, or (3) the presence of incompatible element-enriched inter-granular films. As discussed below, we infer that the inclusions are the major contributor to the U-Th-Ra isotopic heterogeneity and trace phases have not been observed. Nevertheless, inter-granular films may be important for explaining the ^{238}U - ^{234}U

disequilibria. One piece of evidence for the role of inter-granular films for xenolith GN9911 is the ^{234}U excesses observed in the low U concentrations phases. If films containing higher levels of U are in close contact with such phases they would become enriched in ^{234}U due to the effects of recoil.

The preceding section also raises the question of whether inter-granular films might be responsible for the U-Th-Ra disequilibria. However, several observations by Hiraga et al. (2007) would seem to mitigate this possibility: (1) their calculations show that the volume of inter-granular films are too small to result in significant inter-element fractionation; (2) we observe ^{230}Th excesses in all minerals except the relatively inclusion-free orthopyroxene, whereas their theoretical calculations predict enrichment of U over Th in inter-granular films; and (4) they predict that inter-granular films will show enrichment of Ra over Th, yet we observe both excesses and deficits of ^{226}Ra relative to ^{230}Th . Thus, whilst inter-granular films may be important for recoil-derived ^{238}U - ^{234}U disequilibria, they cannot explain the extreme and opposite senses of ^{238}U - ^{230}Th and ^{226}Ra - ^{230}Th disequilibria we observe. In conclusion, we attribute much of the observed U-Th-Ra isotope heterogeneity to the presence of the inclusions.

5.2. *Inferred compositions of the inclusions*

It seems very likely that majority of the heterogeneity in the data arises from variations in the proportion and/or composition of the fluid and melt inclusions in the minerals (e.g., Andersen et al., 1984). Despite this variability, only a few of the analysed minerals have an isotopic composition that lies close to secular equilibrium and there is a general consistency in the sense of the U-series disequilibria. Clearly, the minerals do not form U-Th isochrons (see Fig. 5) and are not equilibrated with respect to U-Th-Ra isotopes, just as they are not in Sr-Nd-Pb isotopic equilibrium (Stolz and Davies, 1988).

Comparison of the results from the relatively inclusion-free and inclusion-rich separates indicates that the U, Th and Ra concentrations in the relatively inclusion-free separates are not always lower than those in the inclusion-rich separates. In contrast, the isotopic comparisons between the relatively inclusion-free and inclusion-rich separates are more systematic with the implication that concentrations and isotopic ratios are not always coupled. This may not be surprising given that the inclusions themselves have several different components (e.g., silicate melt, carbonatite melt, fluids). In detail, the inclusion-rich clinopyroxenes and amphiboles have 3-53% ^{230}Th excesses and 15-50% ^{226}Ra deficits, respectively (see Fig. 5). This is broadly similar to the results from the relatively inclusion-free amphiboles whereas the relatively inclusion-free clinopyroxenes have $\sim 5\%$ ^{230}Th excess and $\sim 74\%$ ^{226}Ra excess. Thus, for the clinopyroxenes, the relatively inclusion-free grains have the opposite sense of ^{226}Ra disequilibria to the bulk separates, indicating that the melts/fluids responsible for the inclusions have ^{230}Th excesses combined with ^{226}Ra deficits, similar to the amphiboles. At least for GN9911, this would suggest that the U-series disequilibria in the amphibole is mostly controlled by the inclusions, consistent with its low U-Th contents and U/Th ratio.

In contrast, whereas the non-leached bulk orthopyroxene separate from Gnotuk has ^{230}Th excess, the relatively inclusion-free separate has a ^{230}Th deficit. We also conducted a leaching experiment on the initial orthopyroxene separate (Table 2) and that analysed at UC Davis (Table 3) was also leached. The leached orthopyroxene separate analysed at Macquarie yielded 4% ^{230}Th excess similar to the original bulk analysis whereas the leachate had a 22% ^{230}Th deficit. However, the U and Th concentrations in the leached separate and the leachate are both similar to each other and to the original separate. In contrast, the UC Davis analysis of a second, leached orthopyroxene separate yielded a 50% ^{230}Th deficit. Consequently, the leaching experiments did not help to resolve the variations but did indicate that the heterogeneous disequilibria signals may be intrinsic to the minerals. Due to their very low U and Th concentrations the orthopyroxenes would have been highly sensitive to any metasomatic addition. Thus, one explanation for the highly variable

orthopyroxene data is a complex one in which there were at least two generations of orthopyroxene that formed from different episodes of infiltration by components that had opposite senses of U-Th disequilibrium! Alternatively, the orthopyroxenes formed at the same time but different generations of fluid/melt inclusions were emplaced by fracturing and fluid flow during metasomatism, some carbonatitic, some silicate. All orthopyroxene analyses yielded ^{226}Ra excesses ranging from 90 to 800%.

6. Origins of the U-series signatures

The U-series systematics of these xenoliths are demonstrably extremely complex. In principle, there are a number of alternative explanations for the origins of the apparent U-series disequilibria in the xenoliths that include surficial alteration, host lava contamination, partial melting during ascent, steady-state diffusion and recent metasomatism. We will discuss each of these in turn.

Since only pristine mineral separates were analysed it seems implausible that the majority of the disequilibria reflect surficial alteration and, as discussed above, a number of general observations mitigate this possibility. Moreover, previous studies found no difference in $^{86}\text{Sr}/^{87}\text{Sr}$ ratios between leachates and residues of mineral separates in other xenoliths from the same locality, suggesting negligible post-entrainment contamination of the xenoliths (Stolz and Davies, 1988). Since Ra should behave similarly (chemically) to Sr, this suggests minimal effect on Ra either.

Another possible explanation for the disequilibria is contamination by the host lavas. However, this also seems precluded by a variety of observations. First, although small amounts of interstitial glass have been observed in similar xenoliths from localities nearby, this glass does not resemble the host lavas. Rather, such glass has interpreted to reflect either (1) infiltration of metasomatic melt (Draper and Green, 1997) or (2) in-situ melting of amphibole/phlogopite during ascent (Yaxley and Kamenetsky, 1999). Our xenoliths were chosen on the basis of a visual absence

of evidence for in-situ melting or amphibole breakdown. Second, previous studies have shown that the U concentrations in the minerals are too high to have been in equilibrium with a basaltic melt (Kleemann et al., 1969). Third, the Sr, Nd and Pb isotope signatures of the xenoliths are distinct from those of their host lavas (McDonough and McCulloch, 1987). Finally, the U-series disequilibria in the Bullenmerri host basalt, tuff and equivalents from Mount Gambier and Mount Schank (Demidjuk et al., 2007), are characterised by near equilibrium ($^{226}\text{Ra}/^{230}\text{Th}$) and U-Th isotope ratios that are distinct from those exhibited by the xenoliths (see Fig. 5). To fractionate two trace elements, the melt/rock ratio in reactive flow has to be on the order of the distribution coefficient for the more compatible of the two elements, or smaller. It seems implausible that such a low melt/rock ratio could be attained on the length scale of a xenolith within the very short (hours to days) duration permitted for entrainment and eruption (cf. Scarfe and Brearley, 1987) when the host magmas represent 3-6% partial melt bearing little ^{226}Ra - ^{230}Th disequilibrium (Demidjuk et al., 2007).

The formation of small patches of melt by amphibole breakdown during decompression (Yaxley and Kamenetsky, 1999) would undoubtedly lead to fractionation between some U-series nuclide parent-daughter pairs and resultant disequilibria. As noted above, the inclusions are too small to be analysed and there is a visual absence of interstitial glass in these two xenoliths. Furthermore, partitioning data indicate that amphibole does not significantly fractionate U from Th (Bourdon et al., 2003; Adam and Green, 2006) whereas ^{226}Ra deficits are predicted (based on the behaviour of Ba) to result from equilibrium with residual amphibole (Blundy and Wood, 2003; Adam and Green, 2006). By implication, if decompression melting was the cause of the disequilibria, the pyroxenes should lie close to ^{238}U - ^{230}Th secular equilibrium and the amphiboles should have ^{226}Ra excesses. Thus, our results do not favour an origin of the disequilibria through partial melting of the xenoliths during ascent.

Numerical calculations show that differences in compatibility and diffusion rates could, in principle, lead to U-series disequilibria amongst mantle minerals at steady-state. Specifically, it has

been suggested that amphibole- (or phlogopite-) peridotite might develop steady state ^{226}Ra - ^{230}Th disequilibrium whereby Ra diffuses out of clinopyroxene into amphibole imparting ^{226}Ra excesses in the latter (Feineman and DePaolo, 2003). Assuming that the amphiboles and clinopyroxenes had reached steady-state, the model of Feineman and DePaolo (2003), predicts ($^{226}\text{Ra}/^{230}\text{Th}$) activity ratios of 2.58 and 0.95, in the amphiboles and the clinopyroxenes, respectively. This is in conflict with the observation of ^{226}Ra deficits in both the bulk amphibole separates and the relatively inclusion-free amphiboles and in any case such a process would be unlikely to produce the large ^{226}Ra excess in the orthopyroxene separate. Accordingly, we have some confidence that much of the apparent disequilibria in these xenoliths reflect melt/fluid infiltration or reactive porous flow that occurred *prior* to their transport to the surface.

7. Extremely young metasomatism

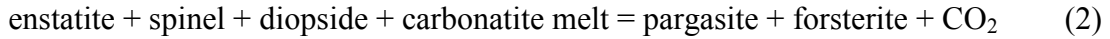
The simultaneous occurrence of both excesses and deficits in both of the ^{238}U - ^{230}Th and ^{230}Th - ^{226}Ra systems within the southeast Australian xenoliths would require a complex, multi-stage history of silicate and carbonatite (and/or CO_2 -rich fluid) metasomatism that we hypothesise to have occurred in-situ within the sub-continental lithospheric mantle. In addition, the ^{226}Ra disequilibria are entirely consistent with several decades of investigation that suggest at least one metasomatic phase in this region involved carbonatite melt and/or melt-wall rock reactions (Green and Wallace, 1988; Yaxley et al., 1998; Porcelli et al., 1992; Matsumoto et al., 2000). All analyses of the orthopyroxene from Gnotuk have significant ^{226}Ra excess. Given that the samples are thought to be several kyr old, this suggests that the metasomatic agent responsible for this signal must initially have had a ^{226}Ra excess of 10 to 50 or more. The only known melts ever found to have this sort of magnitude of disequilibria are carbonatites that can have ($^{226}\text{Ra}/^{230}\text{Th}$) ratios > 60 (Williams et al., 1986; Pyle et al., 1991). The pre-metasomatism protolith, inferred to have been comprised largely of olivine \pm orthopyroxene, would have had very low U and Th concentrations. Such rock would be

highly sensitive to interaction with carbonatite melts that could therefore easily impart very high ($^{226}\text{Ra}/^{230}\text{Th}$) ratios, consistent with the aforementioned independent evidence for carbonatite metasomatism in this region.

In contrast, very large ^{226}Ra deficits are observed in the amphiboles and are inferred for the fluid/melt inclusions in both the amphiboles and the clinopyroxenes. U-Th-Ra partitioning and the effects of daughter nuclide in-growth during decompression result in the vast majority of non subduction-related, mantle-derived melts being characterised by ^{230}Th and ^{226}Ra excesses (Bourdon et al., 2003). To date, ^{226}Ra deficits have only been observed in unusual lavas from Grande Comore, Pitcairn and Tenerife Islands (Claude-Ivanaj et al., 1998; Bourdon and Van Orman, 2009; Turner et al., 2017) and an olivine-melilitite from the Virunga (Condomines et al., 2015) where this signal has been attributed to the presence of hydrous phases (amphibole or phlogopite) in which Ra is inferred to be more compatible than Th (Blundy and Wood, 2003; Adam and Green, 2006).

It has been experimentally demonstrated that rising carbonatite melts coexist with amphibole lherzolite across the pressure range 3-2.1 GPa but then undergo decarbonation reactions commencing at pressures of 2.1 GPa (Wallace and Green, 1988) corresponding to depths of ~ 60 km. Comparison of experimental phase equilibria with our pressure-temperature estimates for the xenoliths places them in the amphibole lherzolite + vapor field of Wallace and Green (1988), although we note that this estimate is strongly dependent of the local geotherm estimate of Griffin et al. (1984) and steeper geotherms, as inferred for adjacent areas (Tappert et al., 2011), would lead to deeper estimates for their last equilibration. Rising melts from the subjacent convecting mantle would saturate in pargasite at 60 km depth, close to the base of the lithosphere here, and traverse the amphibole lherzolite + carbonatite stability field before reaching the depths of origin of the xenoliths where a vapour phase would coexist with the melts; if the xenoliths have a deeper origin, they would be in equilibrium with amphibole lherzolite + carbonatite (Wallace and Green, 1988). As Green and Wallace (1988) and Draper and Green (1997) have emphasised, neither carbonatite or silicic alkaline melts would face any chemical or thermal obstacle to circulating through and

interacting with harzburgitic mantle. The resultant interaction with surrounding, refractory harzburgite can involve reactions of the sort:



As discussed in detail elsewhere, the microstructures of the xenoliths, the presence of CO₂-rich inclusions and the nature of the clinopyroxene replacement of orthopyroxene are entirely consistent with these sorts of reactions (Yaxley et al., 1998). Moreover, because these reactions are likely to persist over some depth range (Wallace and Green, 1988), rising melts and fluids that react to form clinopyroxene, amphibole and inclusions in the surrounding harzburgitic wall rocks would, themselves, have formed in equilibrium with residual pargasite. This is consistent with the observation that all phases in the xenoliths have low K relative to Ta and the clinopyroxenes are characterised by negative Ba and K anomalies, (Fig. 2) and Rb/Sr and Ti/Eu ratios < bulk silicate Earth (Stolz and Davies, 1988). Because pargasite preferentially partitions Ra over Th, the residual melts are predicted to have major deficits of ²²⁶Ra relative to ²³⁰Th, consistent with the observed disequilibria (see also below).

Our preferred interpretation is illustrated schematically on Fig. 6. Residual harzburgite or dunite, located some distance above the base of the lithospheric mantle, was infiltrated and metasomatised by rising carbonatitic melts (Wallace and Green, 1988). Some of these melts, that had not crystallised significant pargasite, imparted ²²⁶Ra excess bearing inclusions to Th-poor orthopyroxene and produced clinopyroxene via reactions such as (1). The conditions controlling U-Th partitioning in carbonatite liquids are not well understood and some recent experiments on sodic carbonatite do not predict significant U-Th-Ra fractionation (Dasgupta et al., 2009). However, this is inconsistent with observations of natrocarbonatites from Oldoinyo Lengai that have ²³⁸U excesses (Williams et al., 1986; Pyle et al., 1991) similar to those observed in the relatively inclusion-free orthopyroxene. In detail, a recent survey shows that carbonatites exhibit a large range of U/Th ratios (Hoernle et al., 2002) such that some would probably also carry ²³⁰Th excesses such as those

observed in the clinopyroxenes and amphiboles and as inferred for the inclusions. Assuming 3 vol.% of inclusions (Andersen et al., 1984), simple mass balance calculations indicate that the inclusions (and by implication the inferred late infiltrating fluids) may contain ~ 3 ppm U, 1 ppm Th and these U and Th values lie well within the range observed in natural carbonatites (Hoernle et al., 2002). We infer that this on-going infiltration also involved formation of pargasite following reaction (2) and resulted in growth of amphibole and entrapment of inclusions in clinopyroxene characterised by ^{226}Ra deficits. We assume that the majority of the orthopyroxene reacted to produce clinopyroxene and that any residual, jadeite-armoured orthopyroxene would have hosted fewer second-generation inclusions and thus retained its earlier-formed ^{226}Ra excess.

7.1. Qualitative modelling

A lack of constraints on a number of key variables, such as source mineralogy and depth, the relative contributions of potential silicic versus carbonatitic metasomatic components and the true age of the xenoliths, limits detailed modelling of the disequilibria. Given the heterogeneity of the minerals our objective in the following is to explore how the more extreme disequilibria might form on the basis that lesser disequilibria are easier to simulate or could be explained by subsequent decay. On this basis we aim here and in the next section to simulate the more extreme signals in some of the GN9911 minerals.

The fractionation of highly incompatible element ratios approaches the inverse of the ratio of their partition coefficients as the extent of melting (F) becomes increasingly small. Using 1025 °C melt-mineral partition coefficients from Adam and Green (2006) for clinopyroxene, orthopyroxene, and garnet and values from Blundy and Wood (2003) for olivine, we calculate bulk garnet lherzolite distribution coefficients of 0.0014, 0.0009 and 1×10^{-5} for U, Th and Ra, respectively (D_{Ra} was calculated from D_{Ba} following Blundy and Wood, 2003). For a melt fraction of $F = 0.002$ and a source composed of 54% olivine, 17% orthopyroxene, 9% clinopyroxene and 20% garnet this

results in a ($^{230}\text{Th}/^{238}\text{U}$) ratio of 1.54 and a ($^{226}\text{Ra}/^{230}\text{Th}$) ratio of 10, assuming a slow melting rate of $5.5 \times 10^{-7} \text{ kg/m}^3/\text{a}$ and the dynamic melting model of Williams and Gill (1989). Changing the clinopyroxene and garnet modes to 19 and 10%, respectively, yields ($^{230}\text{Th}/^{238}\text{U}$) = 1.1 and ($^{226}\text{Ra}/^{230}\text{Th}$) = 17 but this does not significantly alter the conclusions. The ($^{230}\text{Th}/^{238}\text{U}$) ratio is somewhat lower than that observed in some of the clinopyroxenes and amphiboles and those inferred for the orthopyroxene inclusions on Fig. 5. However, the extent of disequilibria would be enhanced by any ^{230}Th in-growth that occurred during melt migration (i.e. reactive porous flow). For infinitesimally small ($F \sim 1 \times 10^{-5}$) melt fractions ($^{230}\text{Th}/^{238}\text{U}$) and ($^{226}\text{Ra}/^{230}\text{Th}$) approach 1.6 and 89, respectively. These results simulate stage 1 on Fig. 6 and plausibly explain the large ^{226}Ra excess in the Gnotuk orthopyroxene.

In contrast, similar melt fractions in equilibrium with residual pargasite, predicted to form as the melts ascended shallower than 65 km, are calculated to have a ($^{230}\text{Th}/^{238}\text{U}$) ratios of ~ 1.11 and a ($^{226}\text{Ra}/^{230}\text{Th}$) ratio of 0.23. Such values can simulate stage 2 on Fig. 6 and plausibly reproduce the compositions inferred for the inclusions in the clinopyroxenes and amphiboles on Fig. 5. These illustrative calculations suggest that metasomatic melt/fluid infiltration and associated pargasite saturation can account for the disequilibria observed in the amphiboles and inferred for the melt inclusions.

7.2. Quantitative modelling

We have attempted to model the U-series observations quantitatively although one complication is that they cannot be modelled by simply assuming equilibrium. For example, if the amphibole and clinopyroxene were in chemical equilibrium, the ^{226}Ra content of the amphibole should be greater than that of the clinopyroxene since D_{Ra} in amphibole is greater than D_{Ra} in clinopyroxene. Blundy and Wood (2003) predicted that $D_{\text{Ra}}/D_{\text{Ba}}$ will range between 0.01 and 0.07 for clinopyroxene while it should be approximately 0.08 for amphibole. Thus, Ra/Ba in amphibole

should be greater than in clinopyroxene. However, the opposite is observed, which means that Ra is not in chemical equilibrium between these two phases (as noted earlier). In addition, the Ba concentration in the amphibole is, as expected, enriched compared with the clinopyroxene. This is also true for other trace elements that typify the amphibole signature, which means that the amphibole has not inherited its trace element content from the phase from which it formed, as indicated by the reactions mentioned above (cf. Johnson et al., 1990). The consequence is that the most recent signature imparted in the ^{226}Ra - ^{230}Th system is inconsistent with the clinopyroxene data and known partitioning of Ra-Th. In other words, the amphibole must have formed under disequilibrium conditions.

In order to explore these considerations more explicitly and to provide some theoretical basis for future studies, we initially calculate the more extreme U-series nuclide distribution among the minerals present in GN9911 assuming simple equilibrium partitioning and secular equilibrium of the ^{238}U -series decay chain. The following equations can be written for mineral phase i:

$$C_i = \frac{C_{tot}}{X_i + \sum_{j \neq i} X_j D_j / D_i} \quad (3)$$

where X_i and D_i represent the mass fraction and mineral/melt partition coefficient of phase i for the element considered and C_{tot} is the initial concentration prior to metasomatism.

If this xenolith undergoes subsequent metasomatism the new equilibrium concentrations in mineral phase i after re-equilibration among the mineral phases will be:

$$C_i^{eq} = \frac{(1-f)C_{tot} + fC_s / (D_m + F(1-D_m))}{X_i + \sum_{j \neq i} X_j D_j / D_i} \quad (4)$$

where f is the mass fraction of metasomatising melt and C_s the concentration in the mantle source of the metasomatic melt. F is the degree of melting of this source and D_m the partition coefficient during melting.

An alternative model is that, instead of achieving chemical equilibrium with the minerals, the metasomatic component is only present in the form of melt inclusions. In this case, a standard mixing equation is applicable:

$$C_i = C_i^{eq} (1 - X_{meta}) + C_{meta} X_{meta} \quad (5)$$

These equations were used to interrogate the results reported in Table 2 and Fig. 4. We first explored the possibility that the minerals in the xenoliths were in chemical equilibrium with respect to the U-series nuclides using equation (3). As shown on Fig. 7, it is clear that none of the observations can be explained with this model.

We next assumed that the xenoliths have been metasomatized by a carbonatite using equation (4) to describe this process. While this model could explain some features of GN9911, it cannot account for the difference between the inclusion-free mineral separates and the inclusion-bearing mineral fractions. In addition, it cannot explain the ^{226}Ra deficit observed in the amphibole. Since carbonatite melts are characterized by ^{226}Ra excesses, equilibration of amphibole with carbonatite should lead to a ^{226}Ra excess in the amphibole since $D_{\text{Ra}}^{\text{amphibole}} > D_{\text{Th}}^{\text{amphibole}}$ (cf. Blundy and Wood, 2003; Adam and Green, 2006).

As suggested above, the observations can be explained by an additional type of metasomatism involving a silicate melt whose composition was modified by the equilibration with residual amphibole (Fig. 6). We used equation (5) to model this second-stage process that can explain the U-series observations for GN9911 nodule, at least from a semi-quantitative viewpoint (Fig. 7). The large ^{226}Ra excess found in the orthopyroxene results from the first stage of carbonatite metasomatism and it seems to have been little affected by the second stage according to our mass balance calculations (and observations). In contrast, the clinopyroxene preserves signatures from both types of metasomatism. The subsequent silicate metasomatic melt, produced in equilibrium with amphibole is characterized by a ^{230}Th excess relative to ^{238}U and a ^{226}Ra deficit relative to ^{230}Th . Consequently, the inclusion-rich minerals show mixing trend towards those

characteristics (see Figs. 5, 7). As noted above, the ^{226}Ra - ^{230}Th systematics of the amphibole indicate an absence of equilibrium with clinopyroxene and to account for this observation, decrease the D_{Ra} for amphibole. The reason for this is not easily understood and remains to be investigated further but it may be that there was diffusive loss of Ra to a melt or fluid phase that favored Ra over amphibole.

Many outstanding questions remain and more sophisticated petrogenetic models could be developed. However, irrespective of what model is ultimately invoked, the half-lives involved indicate that some metasomatism occurred only a few kyr ago and was potentially on-going at the time the xenoliths were entrained by their host basalts and perhaps a precursor to magmatism (Menzies and Murthy, 1980). We hope that this preliminary set of analyses and modelling will encourage further investigations of mantle xenoliths.

8. Wider implications

The incentive to explore for U-series disequilibria in ~ zero-aged mantle xenoliths was, in part, motivated by a desire to try to isolate primary mantle U-series signatures (see also Turner et al., 2012). However, it seems likely that we have contributed to the understanding of mantle metasomatism by demonstrating that, at least in one place, the sub-continental lithospheric mantle has recently been infiltrated by small melt fractions. While the Ra-Th disequilibria does indicate fractionation within the last few millennia, the observation of a large range in ($^{230}\text{Th}/^{232}\text{Th}$) ratios in the mantle minerals (from 0.5 to 3.0) suggests that the some U-Th fractionation took place more than 300 kyr ago and cannot be attributed to a single event responsible for the Ra-Th disequilibrium. This observation is in agreement with the noble gas data that indicate a protracted thermal evolution of the xenoliths.

Overall, the data suggest that the convecting mantle here lay very close to its solidus (cf. Green et al., 2010) over significant time periods such that it could supply very small volume melts to the overlying lithosphere. There is also good evidence for similar processes occurring in the past (see Scott et al., 2014 for a recent example). Because the xenoliths appear to derive from depths some 25 km above the base of the lithosphere in this region (Fishwick et al., 2008; Ford et al., 2010), it would appear that metasomatic melts can circulate at least this far upwards into the lithosphere (cf. Draper and Green, 1997). This indicates that very significant portions of the mantle lithosphere could have experienced metasomatism with significant implications for the effect of recycling such lithosphere into the deep mantle.

The small melt fractions produced as a consequence of the mantle being close to its solidus may be important in lubricating the base of the tectonic plates to facilitate plate movement and may contribute to the seismic low velocity zone (e.g., Karato and Jung, 1998; Hirschman, 2010). Indeed, there is good seismic evidence for the presence of small melt fractions in the lithosphere beneath western Victoria today (Davies and Rawlinson, 2014; Jiang et al., 2016). Our evidence for zero-aged metasomatism also calls into question the long-standing practice in xenolith studies of using long-lived radiogenic isotopes (e.g., Nd isotope model ages) to date metasomatic events (cf. Arndt and Goldstein, 1987). It now seems clear that these ages could reflect the composition of the metasomatic component itself. In the present case, inferred early Phanerozoic Nd model ages (Griffin et al., 1988) probably have little meaning and may even simply reflect metasomatism by carbonatite derived from peridotite with a relatively unmodified, primitive mantle isotopic signature. In other words, the model ages could be due to metasomatism by a component with a distinct Nd isotopic signature rather than reflecting the age of metasomatism itself.

If returned to the asthenosphere by convective removal (e.g., McKenzie and O'Nions, 1983), the composition of the peridotite sampled by these metasomatised xenoliths, is broadly suitable as a candidate for the source of many ocean island basalts (see Fig. 2). Conversely, the xenoliths provide evidence of the small melt fraction required to explain the light rare earth element enrichment of the

continents (O’Nions and McKenzie, 1988). However, they do not resemble the composition of average continental crust for many elements especially its characteristic depletion in the high field strength elements Nb and Ta relative to the light REE. These must have a separate origin.

Acknowledgements

We are grateful to Will Powell for providing access to some of his PhD materials. Comments from many colleagues over the years have helped to significantly improve the manuscript. This study was supported by a Humboldt Research Award to S.T. and a New Zealand Foundation for Research, Science and Technology post-doctoral Fellowship to M.T. for which we are very grateful. We thank two anonymous reviewers for their encouraging comments that helped to improve the final manuscript.

Author contributions

Don Porcelli first suggested this study in 2003. The analyses were undertaken by Michael Turner, Simon Turner and Kari Cooper. The numerical modelling was performed by Bernard Bourdon. Simon Turner and Michael Turner prepared the manuscript.

References

- Adam, J., Green, T., 2006. Trace element partitioning between mica- and amphibole-bearing garnet ilherzolite and hydrous basanitic melt: 1. Experimental results and the investigation of controls on partitioning behaviour. *Contrib. Mineral. Petrol.* 152, 1-17.
- Adam, J., Green, T.H., Day, R.A., 1992. An experimental study of two garnet proxenite xenoliths from the Bullenmerri and Gnotuk Maars of western Victoria, Australia. *Contrib. Mineral. Petrol.* 111, 505-514.
- Andersen, T., O'Reilly, S.Y., Griffin, W.L., 1984. The trapped fluid phase in upper mantle xenoliths from Victoria, Australia: implications for mantle metasomatism. *Contrib. Mineral. Petrol.* 88, 72-85.
- Arndt, N.T., Goldstein, S.L., 1987. Use and abuse of crust-formation ages. *Geology*, 15, 893-895.
- Barbetti, M., Sheard M.J., 1981. Palaeomagnetic results from Mounts Gambier and Schank, South Australia. *J. Geol. Soc. Aust.* 28, 385-394.
- Birck, J.L., 1986. Precision K-Rb-Sr isotope analysis – application to Rb-Sr chronology. *Chem. Geol.* 56, 73-83.
- Blackburn, G., Allison, G.B., Leaney, F.W.J., 1982. Further evidence on the age of tuff at Mt Gambier, South Australia. *Trans. Roy. Soc. S. Aust.* 106, 163-167.
- Blundy, J., Wood, B., 2003. Mineral-melt partitioning of Uranium, Thorium and their daughters. *Rev. Mineral. Geochem.* 52, 59-123.
- Bourdon, B., Van Orman, J.A., 2009. Melting of enriched mantle beneath Pitcairn seamounts: unusual U-Th-Ra systematics provide insights into melt extraction processes. *Earth Planet. Sci. Lett.* 277, 474-481.
- Bourdon, B., Henderson, G., Lundstrom, C., Turner, S., 2003. Uranium series geochemistry. *Rev. Mineral. Geochem.* 52.

- Chabaux, F., Riotte, J., Dequincey, O., 2003. U-Th-Ra fractionation during weathering and river transport. *Rev. Mineral. Geochem.* 52, 533-576.
- Cheng, H., Edwards, R.L., Hoff, J., Gallup, C.D., Richards, D.A., Asmerom, Y., 2000. The half lives of uranium-234 and thorium-230. *Chem. Geol.* 169, 17-33.
- Claude-Ivanaj, C., Bourdon, B., Allegre, C.J., 1998. Ra-Th-Sr systematics in Grande Comore Island: a case study of plume-lithosphere interaction. *Earth Planet. Sci. Lett.* 164, 99-117.
- Condomines, M., Carpentier, M., Ongendangenda, T., 2015. Extreme radium deficit in the 1957 AD Mugogo lava (Virunga volcanic field, Africa): its bearing on olivine-melilitite genesis. *Contrib. Mineral. Petrol.* 169, 29.
- Cooper, K.M., 2001. Time scales of magma generation, differentiation and storage: constraints from Uranium-238 – Thorium-230 – Radium-226 disequilibria. Ph.D. thesis, University of California, Los Angeles, CA, pp. 222.
- Cooper, K.M., Donnelly, C.T., 2008. ^{238}U - ^{230}Th - ^{226}Ra disequilibria in dacite and plagioclase from the 2004-2005 eruption of Mounts St. Helens. In: D.R. Sherrod, W.E Scott and P.H. Stauffer (eds) *A Volcano Rekindled: The Renewed Eruption of Mount St. Helens, 2004-2006*. U.S. Geol. Surv. Prof. Paper 1750.
- Dasgupta, R., Hirschmann, M.M., McDonough, W.F., Spiegelman, M., Withers, A.C., 2009. Trace element partitioning between garnet lherzolite and carbonatite at 6.6 and 8.6 GPa with applications to the geochemistry of the mantle and of mantle-derived melts. *Chem. Geol.* 262, 57-77.
- Davies, D.R., Rawlinson, N., 2014. On the origin of recent intraplate volcanism in Australia. *Geology* doi:10.1130/G36093.1.
- De Deckker, P., 1982. Holocene ostracods, other invertebrates and fish remains from cores of four maar lakes in southeastern Australia. *Proc. R. Soc. Vic.* 94, 183-220.

- Demidjuk, Z., Turner, S., Sandiford, M., George, R., Foden, J., Etheridge, M., 2007. U-series isotope and geodynamic constraints on mantle melting processes beneath the Newer Volcanic Province in South Australia. *Earth Planet. Sci. Lett.* 261, 517-533.
- DePaolo, D.J., Wasserburg, G.J., 1976. Inferences about magma sources and mantle structure from variations in $^{143}\text{Nd}/^{144}\text{Nd}$. *Geophys. Res. Lett.* 3, 743-746.
- Draper, D.S., Green, T.H., 1997. P-T phase relations of silicic, alkaline, aluminous mantle-xenolith glasses under anhydrous and C-O-H fluid-saturated conditions. *J. Petrol.* 38, 1187-1224.
- Feineman, M.D., DePaolo, D.J., 2003. Steady-state ^{226}Ra - ^{230}Th disequilibria in mantle minerals: implications for melt transport rates in island arcs. *Earth Planet. Sci. Lett.* 215, 339-355.
- Firth, C., Handley, H., Turner, S., Cronin, S., Smith, I., 2016. Variable conditions of magma storage and differentiation with links to eruption style at Ambrym volcano, Vanuatu. *J. Petrol.* 57, 1049-1072.
- Fishwick, S., Heintz, M., Kennett, B.L.N., Reading, A.M., Yoshizawa, K., 2008. Steps in lithospheric thickness within eastern Australia, evidence from surface wave tomography. *Tectonics* 27, doi:10.1029/2007TC002116.
- Ford, H.A., Fischer, K.M., Abt, D.L., Rychert, C.A., Elkins-Tanton, L.T., 2010. The lithosphere-asthenosphere boundary and cratonic lithospheric layering beneath Australia from Sp wave imaging. *Earth Planet. Sci. Lett.* 300, 299-310.
- Frey, F.A., Green, D.H., 1974. The mineralogy, geochemistry and origin of lherzolite inclusions in Victorian basanites. *Geochim. Cosmochim. Acta* 38, 1023-1059.
- Frey, F.A., Green, D.H., Roy, S.D., 1978. Integrated models of basalt petrogenesis: a study of quartz tholeiites to olivine melilitites from southeastern Australia utilising geochemical and experimental petrological data. *J. Petrol.* 19, 463-513.
- Green, D.H., Wallace, M.E., 1988. Mantle metasomatism by ephemeral carbonatite melts. *Nature* 336, 459-462.

- Green, D.H., Hibberson, W.O., Kovacs, I., Rosenthal, A., 2010. Water and its influence on the lithosphere-asthenosphere boundary. *Nature* 467, 448-451.
- Griffin, W.L., Wass, S.Y., Hollis, J.D., 1984. Ultramafic xenoliths from Bullenmerri and Gnotuk Maars, Victoria: petrology of a sub-continental crust – mantle transition. *J. Petrol.* 25, 53-87.
- Griffin, W.L., O'Reilly, S.Y., Stabel, A., 1988. Mantle metasomatism beneath western Victoria, Australia: II. Isotopic geochemistry of Cr-diopside lherzolites and Al-augite pyroxenites. *Geochim. Cosmochim. Acta* 52, 449-459.
- Handler, M.R., Bennett, V.C., Esat, T.M., 1997. The persistence of off-cratonic lithospheric mantle: Os isotopic systematics of variably metasomatised southeast Australian xenoliths. *Earth Planet. Sci. Lett.* 151, 61-75.
- Hirano, N. et al., 2006. Volcanism in response to plate flexure. *Science* 313, 1426-1428.
- Hiraga, T., Hirschmann, M.M., Kohlstedt, D.L., 2007. Equilibrium interface segregation in the diopside-forsterite system II: applications of interface enrichment to mantle geochemistry. *Geochim. Cosmochim. Acta* 71, 1281-1289.
- Hirschmann, M.M., 2010. Partial melt in the oceanic low velocity zone. *Phys. Earth Planet. Int.* 179, 60-71.
- Hoernle, K., Tilton, G., Le Bas, M.J., Duggen, S., Gerbe-Schonberg, D., 2002. Geochemistry of oceanic carbonatites compared with continental carbonatites: mantle recycling of oceanic crustal carbonate. *Contrib. Mineral. Petrol.* 142, 520-542.
- Holden, N.E., 1990. Total half-lives for selected nuclides. *Pure Appl. Chem.* 62, 941-958.
- Jagoutz, E., Carlson, R.W., Lugmair, G.W., 1980. Equilibrated Nd-unequilibrated Sr isotopes in mantle xenoliths. *Nature* 286, 708-710.
- Jiang, C., Yang, Y., Rawlinson, N., Griffin, W.L., 2016. Crustal structure of the Newer Volcanics Province, SA Australia, from ambient noise tomography. *Tectonophysics* 683, 382-392.
- Johnson K.T., Dick H.J.B., Shimizu N., 1990. Melting in the oceanic upper mantle: an ion microprobe study of diopsides in abyssal peridotites, *J. Geophys. Res.* 95, 2661-2678.

- Jones, J.H., Walker, D., Pickett, D.A., Murrell, M.T., Beattie, P., 1995. Experimental investigations of the partitioning of Nb, Mo, Ba, Ce, Pb, Ra, Th, Pa, and U between immiscible carbonate and silicate liquids. *Geochim. Cosmochim. Acta* 59, 1307-1320.
- Karato, S.-i., Jung, H., 1998. Water, partial melting and the origin of the seismic low velocity and high attenuation zone in the upper mantle. *Earth Planet. Sci. Lett.* 157, 193-207.
- Kleeman, J.D., Green, D.H., Lovering, J.F., 1969. Uranium distribution in ultramafic inclusions from Victorian basalts. *Earth Planet Sci. Lett.* 5, 449-458.
- Matsumoto, T., Honda, M., McDougall, I., O'Reilly, S.Y., Norman, M., Yaxley, G., 2000. Noble gases in pyroxenites and metasomatised peridotites from the Newer Volcanics, southeastern Australia: implications for mantle metasomatism. *Chem. Geol.* 168, 49-73.
- McBride, J.S., Lambert, D.D., Greig, A., Nichols, I.A., 1996. Multistage evolution of Australian subcontinental mantle: Re-Os constraints from Victorian mantle xenoliths. *Geology* 24, 631-634.
- McDonough, W.F., McCulloch, M.T., 1987. The southeast Australian lithospheric mantle: isotopic and geochemical constraints on its growth and evolution. *Earth Planet. Sci. Lett.* 86, 327-340.
- McKenzie, D., 1989. Some remarks on the movement of small melt fractions in the mantle. *Earth Planet. Sci. Lett.* 95, 53-72.
- McKenzie, D., O'Nions, R.K., 1983. Mantle reservoirs and ocean island basalts. *Nature* 301, 229-231.
- Menzies, M., Murthy, V.R., 1980. Mantle metasomatism as a precursor to the genesis of alkaline magmas – isotopic evidence. *Am. J. Sci.* 280, 622-638.
- O'Nions, R.K., McKenzie, D., 1988. Melting and continent generation. *Earth Planet. Sci. Lett.* 90, 449-456.
- Porcelli, D.R., O'Nions, R.K., Galer, S.J.G., Cohen, A.S., Matthey, D.P., 1992. Isotopic relationships of volatile and lithophile trace elements in continental ultramafic xenoliths. *Contrib. Mineral. Petrol.* 110, 528-538.

- Powell, W., Zhang, M., O'Reilly, S.Y., Tiepolo, M., 2004. Mantle amphibole trace-element and isotopic signatures trace multiple metasomatic episodes in lithospheric mantle, western Victoria, Australia. *Lithos* 75, 141-171.
- Price, R.C., Nicholls, I.A., Gray, C.M., 2003. Cainozoic igneous activity. In: Birch W. D. ed. *Geology of Victoria*, pp. 361-375. Geological Society of Australia Special Publication 23.
- Putirka, K., 2008. Thermometers and Barometers for Volcanic Systems. *Rev. Mineral. Geochem.* 69, 61-120.
- Pyle, D.M., Dawson, J.B., Ivanovich, M., 1991. Short-lived decay series disequilibria in the natrocarbonatite lavas of Oldoinyo Lengai, Tanzania: constraints on the timing of magma genesis. *Earth Planet. Sci. Lett.* 105, 378-396.
- Rosenbaum, J.M., Zindler, A., Rubenstone, J.L., 1996. Mantle fluids: evidence from fluid inclusions. *Geochim. Cosmochim. Acta* 60, 3229-3252.
- Scarfe, C.M., Brearley, M., 1987. Mantle xenoliths: melting and dissolution studies under volatile-free conditions. In Nixon, P. H., ed., *Mantle xenoliths, Volume 1*: Chichester, John Wiley & Sons, p. 599-608.
- Scott, J.M., Hodgkinson, A., Palin, J.M., Waight, T.E., Van der Meer, Q.H.A., Cooper, A.F., 2014. Ancient melt depletion overprinted by young carbonatitic metasomatism in the New Zealand lithospheric mantle. *Contrib. Mineral. Petrol.* 167, 962-963
- Sims, K.W.W., et al., 2008. An inter-laboratory assessment of the Th isotopic composition of synthetic and rock standards. *Geostand. Geoanal. Res.* 32, 65-91.
- Stolz, A.J., Davies, G.R., 1988. Chemical and isotopic evidence from spinel lherzolite xenoliths for episodic metasomatism of the upper mantle beneath southeast Australia. *J. Petrol. Spec. Vol.* 303-330.
- Sun S-s., McDonough, W.F., 1989. Chemical and isotopic systematics of oceanic basalts: implications for mantle composition and processes. *Geol. Soc. Spec. Publ.*, 42, 313-345.

- Tappert, R., Foden, J., Muehlenbachs, K., Wills, K., 2011. Garnet peridotite xenoliths and xenocrysts from the Monk Hill kimberlite, South Australia: insights into the lithospheric mantle beneath the Adelaide Fold Belt. *J. Petrol.* 52, 1965-1986.
- Turner, S., Hawkesworth, C., Rogers, N., Bartlett, J., Worthington, T., Hergt, J., Pearce, J., Smith, I., 1997. ^{238}U - ^{230}Th disequilibria, magma petrogenesis and flux rates beneath the depleted Tonga-Kermadec island arc. *Geochim. Cosmochim. Acta*, 61, 4855-4884.
- Turner, S., Bourdon, B., Hawkesworth, C., Evans, P., 2000. ^{226}Ra - ^{230}Th evidence for multiple dehydration events, rapid melt ascent and the time scales of differentiation beneath the Tonga-Kermadec island arc. *Earth Planet. Sci. Lett.* 179, 581-593.
- Turner, S., Beier, C., Niu, Y., Cook, C., 2011. U-Th-Ra disequilibria and the extent of off-axis volcanism across the East Pacific Rise at 9°30'N, 10°30'N and 11°20'N. *Geochem. Geophys. Geosys.* doi:10.1029/2010GC003403.
- Turner, S., Caulfield, J., Turner, M., van Keken, P., Maury, R., Sandiford, M., Prouteau, G., 2012. Recent contribution of both sediments and fluids to the mantle volatile budget. *Nat. Geosci.*, 5, 50-54.
- Turner, S., Kokfelt, T., Hoernle, K., Johansen, T.S., Hauff, F., Hoernle, K., Lundstrom, C., Bogaard, P. v.d., Klugel, A., 2017. Contrasting magmatic cannibalism in the production of evolved phonolite magmas in the Canary Islands. *Geology*, 45, 147-150.
- Van Otterloo, J., Raveggi, M., Cas, R.A.F., Maas, R., 2014. Ploymagmatic activity at the monogenetic Mt Gambier volcanic complex in the Newer Volcanics Province, SE Australia: new insights into the occurrence of intraplate volcanic activity in Australia. *J. Petrol.* 55, 1317-1351.
- Wallace, M.E., Green, D.H., 1988. An experimental determination of primary carbonatite magma composition. *Nature* 335, 343-346.

- Williams, R.W., Gill, J.B., Bruland, K.W., 1986. Ra-Th disequilibria systematics: timescales of carbonatite magma formation at Oldoinyo Lengai volcano, Tanzania. *Geochim. Cosmochim. Acta* 50, 1249-1259.
- Williams, R.W., Gill, J.B., 1989. Effects of partial melting on the uranium decay series. *Geochim. Cosmochim. Acta* 53, 1607-1619.
- Workman, R.K., Hart, S.R., Jackson, M., Regelous, M., Farley, K.A., Blusztajn, J., Kurz, M. and Staudigel, H. 2004. Recycled metasomatized lithosphere as the origin of the Enriched Mantle II (EM2) end - member: Evidence from the Samoan Volcanic Chain. *Geochemistry Geophysics Geosystems* 5: doi: 10.1029/2003GC000623.
- Yaxley, G.M., Kamenetsky, V., 1999. In situ origin for glass in mantle xenoliths from southeastern Australia: insights from trace element compositions of glasses and metasomatic phases. *Earth Planet Sci. Lett.* 172, 97-109.
- Yaxley, G.M., Green, D.H., Kamenetsky, V., 1998. Carbonatite metasomatism in the southeastern Australian lithosphere. *J. Petrol.* 39, 1917-1930.
- Zhu, W., Gaetani, G.A., Fosseis, F., Montesi, L.G.J., De Carlo, F., 2010. Microtomography of partially molten rocks: three-dimensional melt distribution in mantle peridotite. *Science* 332, 88-91.

Fig. 1. (a) Location map with shaded area indicating the main extent of the Newer Volcanics. (b) Hand specimen of a Bullenmerri metasomatised xenolith showing mild alignment of grains of amphibole (dark) parallel to the arrow. Ruler scale is cm. (c) Photomicrograph of Bullenmerri xenolith showing the fresh, un-altered nature of the xenolith and textures between olivine, clinopyroxene and amphibole (crossed polars; width of view 1.5 mm). Note the numerous fluid inclusions (black).

Fig. 2. Primitive mantle-normalised incompatible trace element diagrams for Lake Bullenmerri and Gnotuk xenoliths. The low K levels relative to Ta in the bulk xenoliths and minerals and low Rb, Ba and Sr relative to REE in the bulk xenoliths and clinopyroxenes which provide one line of evidence for metasomatism by carbonatite melts formed in equilibrium with residual pargasite. Thick grey line depicts an average ocean island basalt Sun and McDonough (1989).

Fig. 3. Plots of (a) ($^{230}\text{Th}/^{238}\text{U}$) versus Th and (b) ($^{226}\text{Ra}/^{230}\text{Th}$) versus Ra. The lack of correlation on both diagrams suggests that the measured disequilibria are not an analytical artefact resulting from the low concentrations (i.e. the disequilibria are not systematically larger in the lower concentration materials).

Fig. 4. Plots of U-Th and Ra-Th disequilibria against ($^{234}\text{U}/^{238}\text{U}$). The effect of alteration by interaction with the Maar lake waters would result in ^{238}U and ^{226}Ra excesses that increase with increasing ($^{234}\text{U}/^{238}\text{U}$) > 1. No such correlation is observed and ($^{230}\text{Th}/^{238}\text{U}$) and ($^{226}\text{Ra}/^{230}\text{Th}$) ratios both greater and less than 1 are observed.

Fig. 5. U-Th equiline and ($^{230}\text{Th}/^{238}\text{U}$) and ($^{226}\text{Ra}/^{230}\text{Th}$) diagrams for the Bullenmerri and Gnotuk xenoliths. Circles are clinopyroxene, squares are amphibole and triangles are orthopyroxene. Filled and open symbols represent bulk and relatively inclusion-free separates, respectively. Thus, the

inferred composition of the inclusions (incl.) lie on a projection from the open symbols through the filled symbols as indicated by the grey dashed arrows. Except for the orthopyroxene from GN9911, there is a general consistency that the inclusions, and thus inferred metasomatic melts, have ^{230}Th excess combined with ^{226}Ra deficit (see text for discussion). The Bullenmerri host basalt (B) and Tuff (T) are also shown (the basalt lies off the right side of the lower panel). Grey field shows the range of disequilibria in basalts from Mounts Gambier and Schank (Demidjuk et al., 2007). Dashed black lines represent secular equilibrium. Error bars are smaller than the symbol sizes.

Fig. 6. Illustration of the metasomatic model. Stage 1: carbonatite infiltration of lithospheric harzburgite imparts ^{226}Ra excess in orthopyroxene and produces jadeite via reactions similar to (1). Available carbonatite U-Th data suggest that this could produce either sense of U-Th disequilibrium. Stage 2: decarbonation reactions lead to precipitation of pargasite and impart ^{226}Ra deficit coupled with ^{230}Th excess preserved in the melt inclusions (see main text for discussion). The large range in ($^{230}\text{Th}/^{232}\text{Th}$) ratios in the minerals suggests that an older event of ^{238}U - ^{230}Th fractionation pre-dated that responsible for ^{226}Ra - ^{230}Th disequilibrium.

Fig. 7. Results of quantitative modelling of metasomatism in the GN9911 xenolith. The stars show the U-series composition of minerals in equilibrium with each other, using equation (3) and clearly cannot explain the observations. The curves show mixing calculations between a mineral assemblage that was first metasomatised by a carbonatitic melt, assuming a mass fraction of 3%, and then metasomatized to variable degree by a silicic melt (see text for details of the model and the equations used). In this model, the melt mass fractions range from 0 to 10%. This model can broadly reproduce the observations of ^{226}Ra - ^{230}Th and ^{230}Th - ^{238}U disequilibria in the minerals. The carbonatite melt and silicic melt compositions used in this model were within the range of those calculated in the text. The mineral – silicate melt partition coefficients were those cited in the text, except for those for amphibole whose partition coefficients need to “tuned-down” to explain their

low U-Th contents (see text for discussion). The mineral – carbonatite partition coefficients were calculated using the silicate – carbonatite partition coefficients of Jones et al. (1995). The mode of the minerals phases were taken from Powell et al. (2004).

Table 1. Major and trace element analyses of bulk xenoliths, mineral separates and host lavas

Sample	BM Host basalt	BM tuff	BM993 bulk xenolith	BM993 cpx	BM993 amph	GN Host basalt	GN9911 bulk xenolith	GN9911 cpx	GN9911 amph	GN9911 opx
SiO ₂	45.74	-	44.36	53.40	43.72	45.16	44.76	52.52	43.09	55.75
TiO ₂	3.32	-	0.34	0.25	1.61	2.47	0.05	0.27	1.45	0.05
Al ₂ O ₃	15.49	-	3.00	4.51	12.92	13.95	2.84	4.76	14.83	3.31
Fe ₂ O ₃	12.80	-	8.67	3.00	4.22	11.87	8.61	2.66	3.69	6.75
MnO	0.14	-	0.13	0.07	0.04	0.16	0.12	0.04	0.05	0.13
MgO	6.54	-	39.24	15.47	17.51	6.71	41.45	15.69	18.13	34.48
CaO	8.74	-	2.91	20.11	10.55	6.89	2.50	21.99	11.36	0.43
Na ₂ O	5.08	-	0.63	1.86	3.48	5.74	0.24	1.41	3.78	0.06
K ₂ O	2.22	-	0.20	0.00	1.09	3.05	0.01	0.01	0.27	0.00
P ₂ O ₅	1.19	-	0.03	-	-	1.09	0.01	-	-	-
Total	101.26	-	99.51	98.67	95.14	97.09	100.59	99.35	96.65	100.96
Be	3.6	2.9	0.29	-	-	-	0.05	-	-	-
Sc	14.0	13.0	14.8	57.9	37.8	-	13.6	71.0	52.0	-
V	153.0	0	85	128	184	-	78	201	315	-
Cr	174.0	3	3165	-	-	-	2977	-	-	-
Co	55.0	35.0	101.5	14.0	27.0	-	106.1	13.0	29.0	-
Ni	249.0	0	1767	220	568	-	1887	217	679	-
Cu	32.0	28.0	3.0	-	-	-	1.8	-	-	-
Zn	129.0	9	51.5	-	-	-	62.2	-	-	-
Ga	22.0	18.7	4.9	-	-	-	2.2	-	-	-
Rb	25.0	43.0	1.7	0.0	4.9	-	0.2	-	2.4	-
Sr	709.0	0	99	89	175	-	11	46	102	-
Y	27.3	22.8	3.9	10.0	12.0	-	2.3	15.0	25.0	-
Zr	380.0	5	76	190	213	-	4	20	26	-
Nb	85.3	51.0	12.2	0.7	64.0	-	1.0	0.3	48.0	-
Mo	2.47	0.81	0.49	-	-	-	0.45	-	-	-
Cd	0.17	0.12	0.230	-	-	-	0.100	-	-	-
Cs	0.43	2.26	0.02	-	-	-	0.01	-	-	-
Ba	442	226	56	1	199	-	3	-	128	-
La	56.42	4	4.6	10.6	14.7	100	0.5	2.7	4.2	-
Ce	114.17	6	8	21	29	186	1	5	8	-
Pr	13.84	9.23	1.1	2.9	3.7	-	0.1	0.8	1.2	-
Nd	53.62	3	5.3	12.6	16.1	77.4	0.6	4.0	6.2	-
Sm	10.92	7.03	1.2	2.9	3.7	14.3	0.2	1.3	2.0	-
Eu	3.30	1.86	0.38	0.94	1.20	4.43	0.08	0.49	0.77	-
Gd	9.08	5.90	0.97	2.84	3.48	11.5	0.26	1.87	3.03	-

Tb	1.28	0.85	0.14	-	-	-	0.05	-	-	-
Dy	5.94	5.90	0.79	2.31	2.76	7.43	0.37	2.55	4.28	-
Ho	1.00	0.77	0.14	0.41	0.48	-	0.09	0.56	0.99	-
Er	2.25	1.93	0.36	1.03	1.20	2.64	0.27	1.72	2.83	-
Yb	1.45	1.51	0.30	0.91	0.97	1.59	0.28	1.63	2.60	-
Lu	0.18	0.21	0.040	0.120	0.130	-	0.050	0.233	0.348	-
Hf	7.82	6.44	2.55	6.90	7.13	-	0.10	0.58	0.75	-
Ta	5.09	2.99	1.01	0.15	6.51	-	0.04	0.10	2.87	-
Pb	5.73	9.93	1.30	-	-	-	0.85	-	-	-

Table 2. U-Th-Ra disequilibria data for western Victorian mantle xenoliths and eruptive host products

Location and type	Sample	U (ppm)	Th (ppm)	²²⁶ Ra (fg/g)	(²³⁴ U/ ²³⁸ U)	(²³⁸ U/ ²³² Th)	(²³⁰ Th/ ²³² Th)	(²³⁰ Th/ ²³⁸ U)	(²²⁶ Ra/ ²³⁸ U)
Lake Bullenmerri	Host basalt	1.013	7.471	567	1.023	0.411	0.729	1.774	0.93
	Tuff	1.115	8.645	405	0.885	0.391	0.391	1.000	1.07
<i>Bulk mineral separates (2006):</i>									
Lake Bullenmerri	BM993 cpx	0.195	1.293	81	1.007	0.457	0.649	1.418	0.86
	<i>Duplicate*</i>	0.245	1.272	86	0.933	0.584	0.618	1.058	0.77
Lake Bullenmerri	BM993 amph	0.396	0.571	106	1.014	2.102	2.875	1.367	0.57
Lake Gnotuk	GN9911 cpx	0.162	0.611	6	1.014	0.806	0.818	1.015	0.10
	<i>Duplicate*</i>	0.163	0.596	47	0.976	0.828	1.279	1.545	0.56
Lake Gnotuk	GN9911 opx	0.012	0.047	47	1.023	0.775	0.911	1.175	9.73
	<i>Leached*</i>	0.015	0.040	-	0.994	1.158	1.213	1.047	-
	<i>Leachate*</i>	0.029	0.033	-	1.018	2.690	2.105	0.783	-
<i>Hand-picked mineral separates with no inclusions (2010):</i>									
Lake Bullenmerri	BM993 cpx	0.245	1.272	152	0.933	0.584	0.618	1.057	1.74
Lake Bullenmerri	BM993 amph	0.295	1.617	92	0.925	0.553	0.591	1.069	0.86
Lake Gnotuk	GN9911 cpx	0.141	0.578	87	0.944	0.740	0.776	1.049	1.74
Lake Gnotuk	GN9911 amph	0.014	0.052	3	1.035	0.806	1.092	1.354	0.47
Lake Gnotuk	GN9911 opx	0.008	0.048	22	1.033	0.513	0.445	0.868	9.38
<i>Av. standard and year*:</i>									
2005	TML-3	10.54	29.61	3447	0.993	1.106	1.087	0.983	0.94
		4	4						
2010	TML-3	10.72	29.44	3513	0.993	1.106	1.077	0.974	0.99
		7	2						
2011	TML-3	10.31	29.03	3533	1.002	1.078	1.082	1.004	1.02
		5	4						
2012	TML-3	10.70	30.12	3578	1.001	1.078	1.082	1.004	0.98
		5	1						

*Duplicates, host basalt and tuff were analysed in 2012
 Errors are 1 standard error

Table 3. U-Th-Ra disequilibria data for minerals analysed at University of California, Davis in 2018

Location	Sample	U (ppm)	Th (ppm)	^{226}Ra (fg/g)	$(^{234}\text{U}/^{238}\text{U})$	$(^{238}\text{U}/^{232}\text{Th})$	$(^{230}\text{Th}/^{232}\text{Th})$	$(^{230}\text{Th}/^{238}\text{U})$	$(^{226}\text{Ra}/^{230}\text{Th})$
Lake Gnotuk	GN9911 cpx	0.157	0.607	50.91	0.997	0.785	0.795	1.013	0.95
Lake Gnotuk	GN9911 opx*	0.015	0.037	4.88	1.006†	1.272	0.629	0.494	1.91
W2-KMC- 2018-1	Standard	0.502	2.175	163.1	1.003	0.700	0.707	1.010	0.95

*Leached in HCl at
Macquarie University

†Average of two instrument runs on
the same solution

Errors are 1 standard error

Highlights:

1. Upper continental mantle materials from western Victoria, Australia preserve U-Th-Ra disequilibria
2. Eruption ages can only be a few kyr
3. Metasomatism in this region is very recent and possibly on-going
4. The subjacent asthenosphere lies close to its solidus

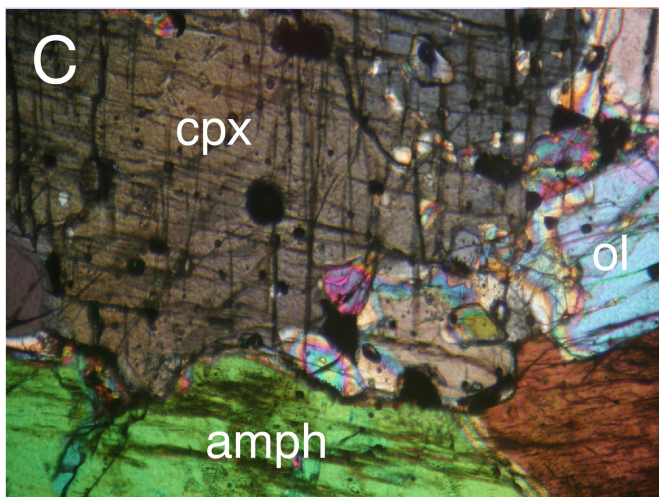
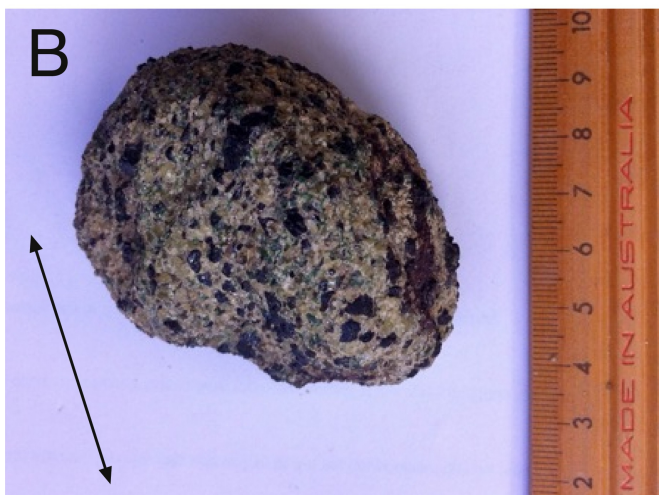
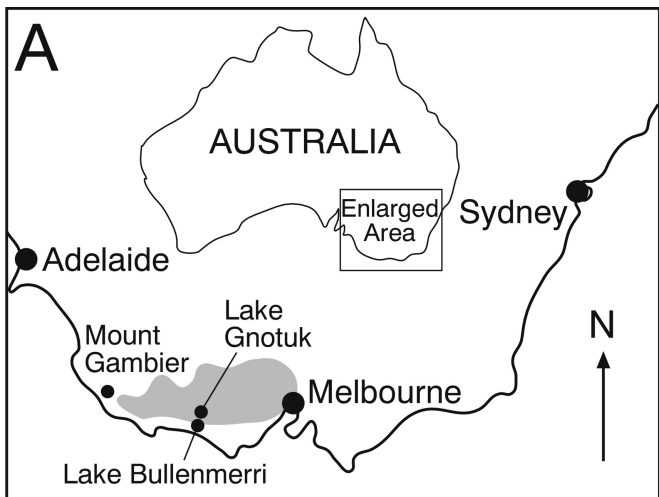


Figure 1

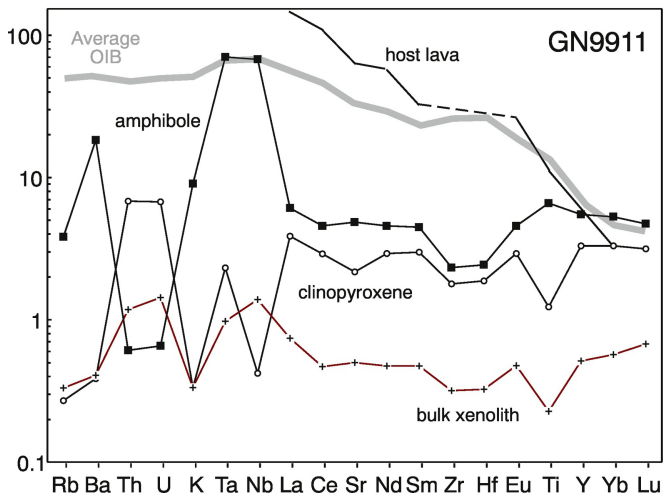
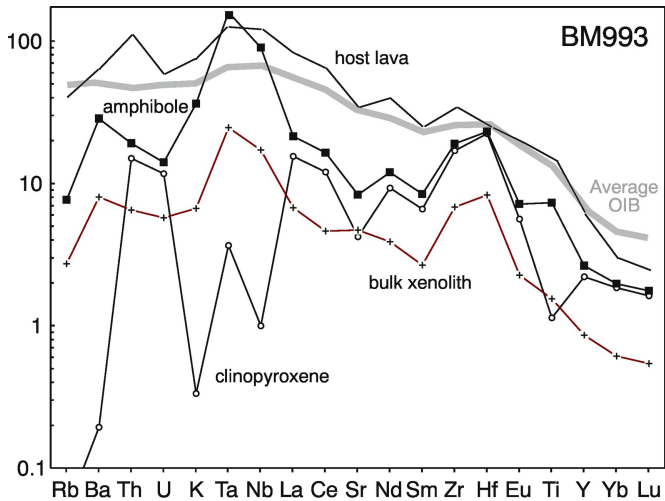


Figure 2

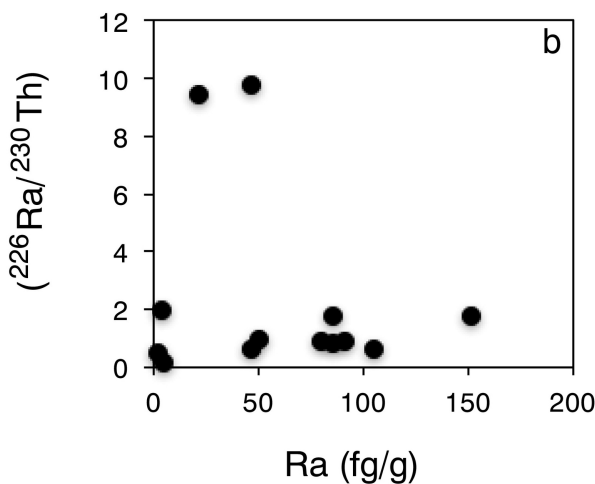
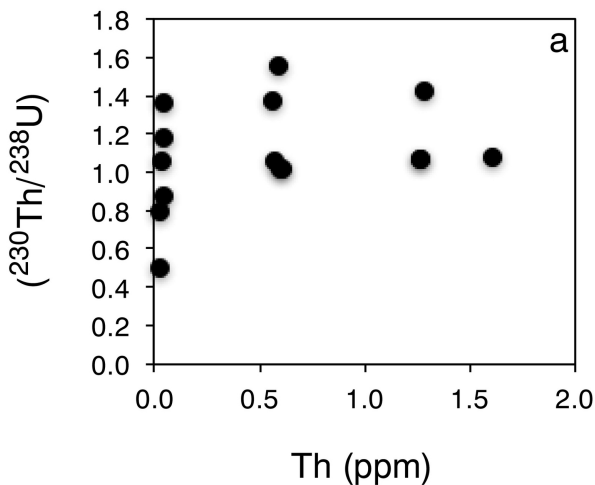


Figure 3

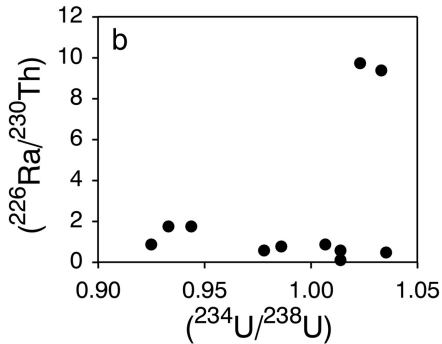
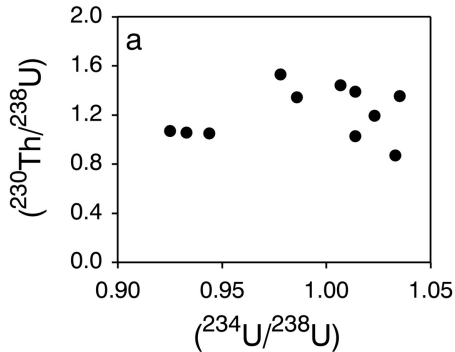
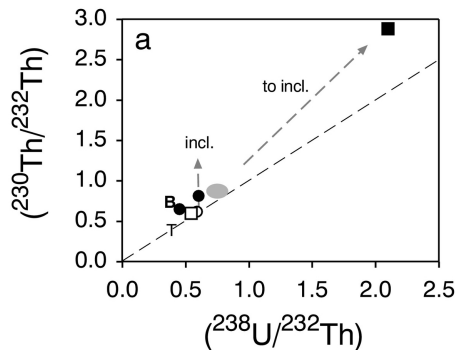


Figure 4

BM993



GN9911

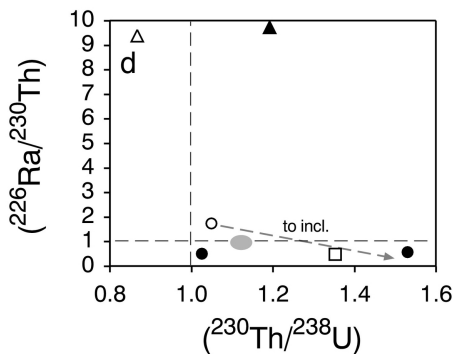
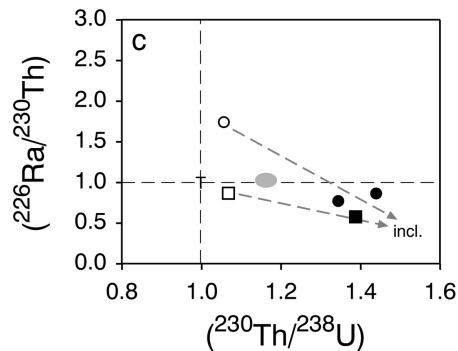
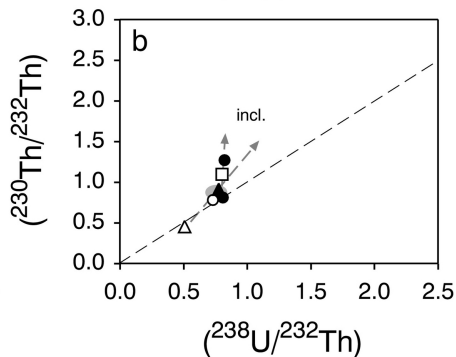
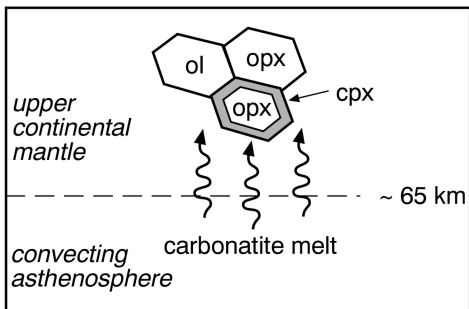


Figure 5

Stage 1



Stage 2

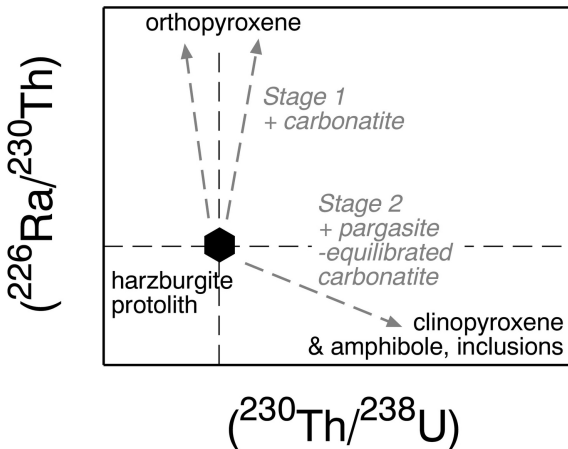
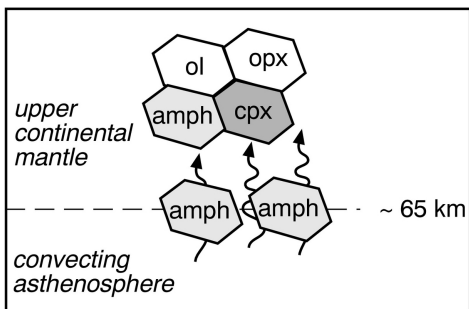


Figure 6

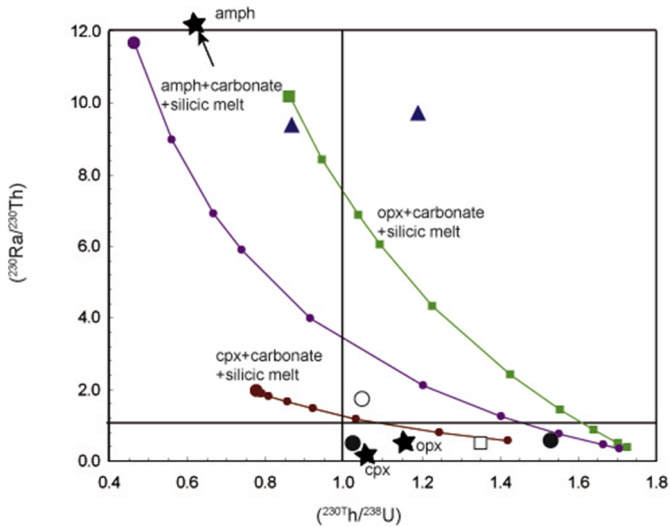


Figure 7